

# Prototype Phased-Array Patch Loop Antennae for Electron Cyclotron Emission Diagnostics<sup>\*)</sup>

Masaharu FUKUYAMA, Hiroshi IDEI<sup>1)</sup>, Miu YUNOKI, Ryuichi ASHIDA, Daichi OGATA, Ryuya IKEZOE<sup>1)</sup> and Takumi ONCHI<sup>1)</sup>

*Interdisciplinary Graduate School of Engineering Sciences, Kyushu University, Kasuga 816-8580, Japan*

<sup>1)</sup>*Research Institute for Applied Mechanics, Kyushu University, Kasuga 816-8580, Japan*

(Received 9 January 2019 / Accepted 9 April 2019)

A two-dimensional (2D) phased-array-antenna (PAA) for electron cyclotron emission is one of the diagnostics for finding the window area of mode conversion from electron cyclotron waves to electron Bernstein wave. Spatial resolution of the reconstructed emission field pattern is improved with a lot of the antenna elements. The study proposes a phased-array patch loop antenna (PAPA) as a promising system to increase the elements of PAA. A 2D image reconstruction of a 6 GHz radio frequency source emission shows that the source position is detected within millimeter range by applying the prototype PAPA. This result indicates that the 2D image reconstruction with multi-element PAPA is feasible.

© 2019 The Japan Society of Plasma Science and Nuclear Fusion Research

Keywords: electron cyclotron emission, phased array antenna, patch antenna, adaptive-array technique

DOI: 10.1585/pfr.14.3402111

## 1. Introduction

A non-inductive method to heat plasma and start-up current solely by electromagnetic waves is required in the spherical tokamaks (STs) with limited space for the central solenoid Ohmic-heating coil. Even though the electromagnetic wave faces its cut-off regarding high plasma density, an electrostatic wave so-called electron Bernstein wave (EBW) can be propagated in such over-dense plasma with no density limits. The obliquely injected ordinary-mode (O-mode) wave from the magnetic low-field side (LFS) would be converted to extra-ordinary-mode (X-mode) wave at the O-mode cut-off layer and then, it is converted to EBW at the upper hybrid resonance. The optimal incident angle for the O-X-mode conversion depends on the external magnetic field and the plasma density. The electrostatic EBW emission can be detected as the electromagnetic wave at LFS by the inverse mode conversion from EBW to O-mode [1].

In Q-Shu University Experiment with steady-state Spherical Tokamak (QUEST), the EBW heating and current drive are performed with major and minor radii as 0.64 m and 0.36 m, respectively. When the O-mode cut-off layer was positioned at a normalized plasma radius  $\rho = 0.78$ , the optimum parallel (to magnetic field) refractive index was evaluated as  $N_{||}^{\text{opt}} = 0.61$  [2]. To search the mode conversion window, the phased-array waveguide antenna (PAWA) has been developed [3]. Then, the low-power experiment with  $3 \times 3$  PAWA was conducted in QUEST ves-

sel [4]. A thermal noise source (NS) mimicking incoherent emission was detected using the adaptive-array technique, and the location of the NS was identified with a two-dimensional (2D) image reconstruction of the emission. Although the way to increase the element of the phased-array antenna (PAA) effectively works to suppress the side lobe and precisely identify the NS location, the fabrication of multiple-PAWA requires complex processes with high cost. Since the patch loop antenna is suitable for mass production due to compact, simple, and lightweight features, the fabrication of multiple-element phased-array patch loop antenna (PAPA) is effective to increase the element of the PAA [5]. This paper demonstrates a 2D image reconstruction using prototype PAPA as the proof-of-principle experiment for the multi-element PAPA.

The rest of this paper is organized as follows. In Section 2, a fabricated patch loop antenna benchmarked for assembling the PAPA is introduced. Section 3 presents test results of the prototype PAPA at low-power facilities, and its 2D emission image reconstruction for finding the location of radio frequency (RF) and emission source (ES) with PAPA. A brief conclusion is given in Section 4.

## 2. Patch Loop Antenna

The patch loop antenna in which the loop is square-shaped was designed for 6 GHz-wave detections by applying a three-dimensional (3D) electromagnetic simulator “COMSOL Multiphysics”. The simulation results show that the patch loop antenna with a quarter-wavelength side has higher antenna gain than that of the eighth-wavelength side. However, the directivity of the quarter-wavelength-

author's e-mail: fukuyama@triam.kyushu-u.ac.jp

<sup>\*)</sup> This article is based on the presentation at the 27th International Toki Conference (ITC27) & the 13th Asia Pacific Plasma Theory Conference (APPTC2018).

side antenna is lower than that of the eighth-wavelength-side antenna. Since antenna gain is relatively low compared to that of waveguide antenna in general, the antenna gain of patch loop antenna as high as possible is required at the patch loop antenna. Thus, an antenna with a quarter-wavelength side was selected. A patch loop antenna was made by milling 1.6 mm thickness FR1. Figure 1 depicts a photo of the fabricated antenna. The performance of this antenna was verified experimentally.

### 2.1 Experiment using one patch loop antenna

The property of a fabricated antenna was tested using a low-power test system. Figures 2 (a) and (b) show a block diagram of the heterodyne system with a patch loop antenna, a launcher antenna, and a patch loop antenna. 6 GHz RF-wave was generated by applying a synthesizer. The RF-wave was launched from a quad-ridge antenna and its radiation field was received by the patch loop antenna on a 3D stage. The propagating-wave fields were measured as a 70 MHz intermediate frequency wave (IF-wave) with a 5.93 GHz local oscillator wave (LO-wave) at the heterodyne detection. As shown in Fig. 2 (a), the reference, 70 MHz IF-wave, was detected before the launcher antenna. Using a two-channel network analyzer, the IF phase of the propagating wave was measured as the dif-



Fig. 1 A photo of the patch loop antenna fabricated by milling 1.6 mm thickness paper phenolic copper clad laminates (FR1). The side of the square loop is about quarter-wave.

ferential phase between the reference and the propagating sides. The RF and LO synthesizers, and the network analyzer were phase-locked using a 10 MHz reference clock signal.

Figures 3 (a) and (b) show the horizontal  $x$ - and vertical  $y$ - phase profiles at the normal propagating distance of  $z = 0.182$  m where the coordinates of  $(x, y, z)$  are illustrated in Fig. 2 (b). The solid lines in Fig. 3 show the calculated phase profiles from the Kirchoff integral at the launcher antenna center with a point image source. Figure 3 (c) illustrates the phase evolution along the propagation  $z$  at

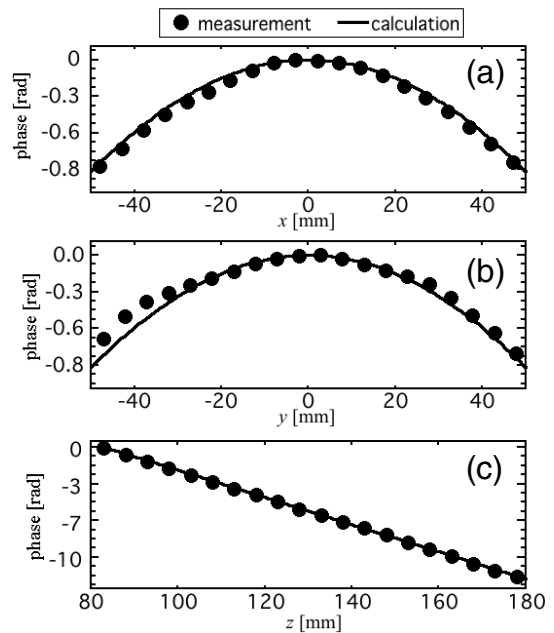


Fig. 3 Measured and calculated phase profiles along  $x$ - and  $y$ -directions, and the evolution in propagating  $z$ -direction with a patch loop antenna. The directions of coordinates  $(x, y, z)$  are illustrated in Fig. 2 (b).

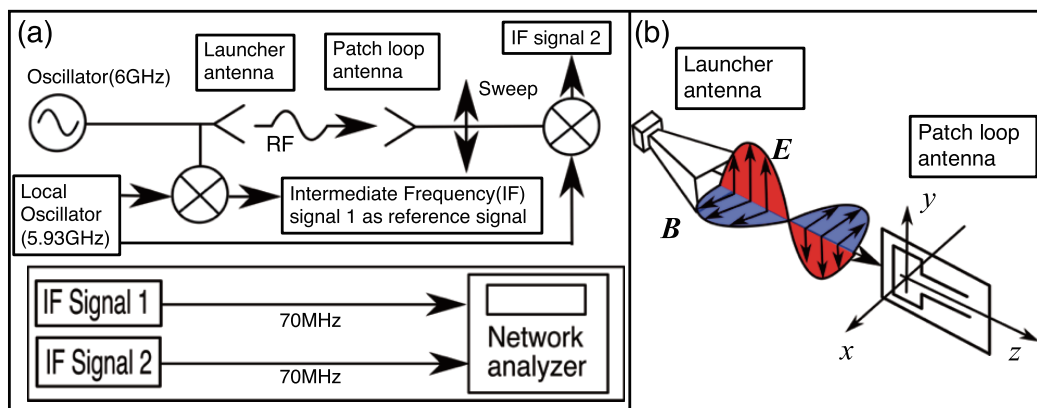


Fig. 2 (a) Block diagram of the heterodyne system with a quad ridged launcher antenna and a patch loop antenna to observe if the patch antenna can properly detect propagating-wave field-phase. Two synthesizers are used to excite test RF-wave and local oscillator (LO) wave at heterodyne detection, with phase-locking using a 10 MHz clock reference signal. (b) Configuration of a launcher antenna and a patch loop antenna for the phase detection with the patch loop antenna. The position of the receiver loop antenna is shifted by movable 3D stage in  $x$ -,  $y$ - and  $z$ -directions for measuring radiated field-phase profiles or evolution.

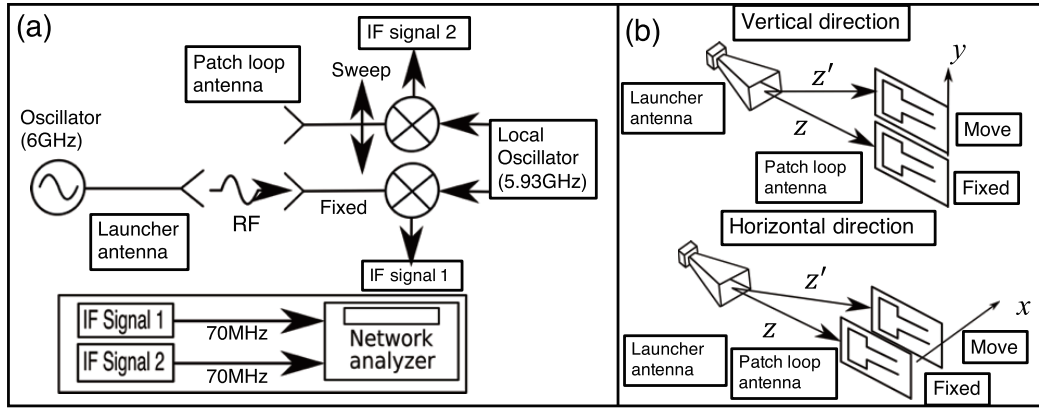


Fig. 4 (a) Block diagram of the heterodyne system with two path loop antennae for checking the interference effect between them. (b) Configuration for checking the interference between the two antennae in phase measurements. The loop antennae are arrayed vertically and horizontally to check the interference in their different directions. The one loop antenna is moved using the 3D stage for the other fixed loop antenna to change the distance between the antennae.

$x = y = 0$ . The origin point was the center of the square loop. As shown in Fig. 3, the profiles and evolution of phase are in good agreement with the calculated results and the expected linear dependence, respectively. These results show that the fabricated patch antenna is present to correctly detect the emitted phase for the adaptive-array analysis.

## 2.2 Experiment with two patch loop antennae

It is important to accurately measure the phase profile and evolution for identifying the ES location through the adaptive-array analysis. Phase measurements would be difficult because of interference when the distance between the two antennae is close. Two patch loop antennae were used to check the interference effect between the antennae. Figure 4 (a) shows a block diagram of the heterodyne system with two antennae for checking the interference effect. The same 6 GHz RF-wave was utilized with the same 5.93 GHz LO-wave. As shown in Fig. 4 (b), these antennae were arrayed vertically and horizontally in their directions to check the interference. One patch loop antenna was fixed and the position of the other antenna was shifted using the 3D stage. The phase difference ( $\Delta\theta$ ) between the antennae was measured using a network analyzer.

$\Delta\theta$  was evaluated as a linear dependence on the differential propagation distance ( $z' - z$ ) between the antennae;  $\Delta\theta = k(z' - z)$ , where  $z'$  denotes the distance between the launcher and the swept antennae defined as  $\sqrt{x^2 + y^2 + z^2}$ . Figure 5 demonstrates the measured  $\Delta\theta$  on ( $z' - z$ ). As shown in Fig. 5 (a), the interference effect between the antennae was not detected in the vertical  $y$ -direction, since the measured  $\Delta\theta$  was linearly proportional to ( $z' - z$ ). However, as shown in Fig. 5 (b), the measured  $\Delta\theta$  was distorted from the calculated line when the ( $z' - z$ ) was smaller than 5 mm in the horizontal  $x$ -direction. When ( $z' - z$ ) = 9.6 mm, *i.e.*, the distance between the antennae is 60 mm, the interfer-

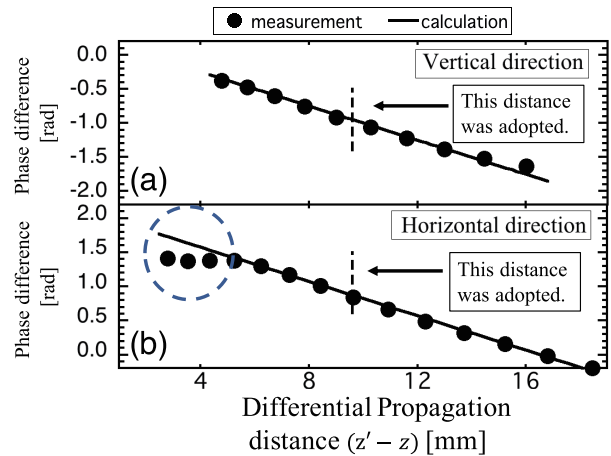


Fig. 5 Dependence of the phase difference ( $\Delta\theta$ ) on differential propagation distance ( $z' - z$ ) between two patch loop antennae, where  $z'$  denotes the distance between the launcher and the swept antennae which can be defined by  $\sqrt{x^2 + y^2 + z^2}$ . The coordinates of ( $x, y, z$ ) are shown in Fig. 4 (b). The marked distance with broken lines of ( $z' - z$ ) = 9.6 mm corresponds to the two antennae distance of 60 mm.

ence effect was not observed even in the  $x$ -direction as well as in the  $y$ -direction, and there was no significant ghost or side lobes on 2D image reconstruction. The configuration with the antenna distance of 60 mm in both  $x$ - and  $y$ -directions has been adopted for the PAPA.

## 3. PAPA

Figure 6 presents a photo of the fabricated four-element PAPA based on the bench test results. Each patch antenna was fixed using sub miniature type a (SMA) cabling. The SMA cables were fixed on acrylic plates. This PAPA comprises four ( $2 \times 2$ ) elements.

### 3.1 Experiment using PAPA

The assembled PAPA for the adaptive array analysis was bench-tested to check accuracy. Figure 7 (a) depicts a block diagram of the heterodyne system with a four-element PAPA. The same RF and LO waves were utilized for the PAPA test. The four-element PAPA was fixed, while the launcher antenna position was shifted in the normal propagating  $z$ -direction using the 3D stage. The phase evolution on  $z'$  for each loop antenna was measured (a total of four times), where  $z'$  denotes the propagation distance between the swept launcher antenna and the PAPA, and it is defined by  $\sqrt{x^2 + y^2 + z^2}$  in the coordinates shown in Fig. 7 (b).

Figure 8 shows each phase evolution of the four-elements on  $z'$  measured at  $x = y = 0$ . Solid lines present the linear dependencies of  $kz'$  for the various antenna elements. The measured phase evolutions on  $z'$  correspond to the linear dependencies. This result shows that the effect of interference is relatively small enough. While phase offsets from the difference in length of RF circuits are not

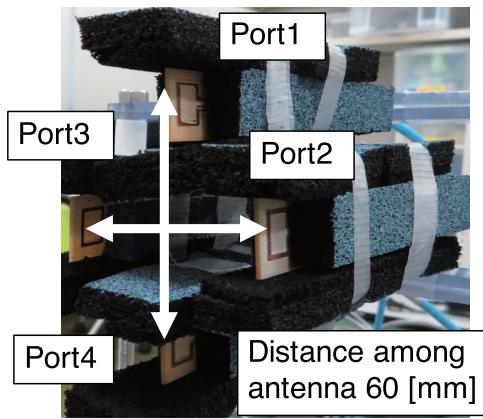


Fig. 6 Photo of fabricated four-element PAPA. The distances between centers of the square loops in horizontal and vertical coordinates are 60 mm along the interference check between the antenna elements described in section 3.1.

negligible. Therefore, calibration to eliminate the offset is recommended. A method for this is given below.

### 3.2 A 2D image reconstruction with PAPA

The 2D image reconstruction was demonstrated with the four-element PAPA to identify the ES location. The beam-forming adaptive-array technique was used to reconstruct the emission pattern. The measured profile of intensity,  $I(x, y)$ , in the beam-forming can be given by

$$I(x, y) = \sum_{i=1}^4 |\exp(\theta_i - \theta_i^{\text{offset}} - k(r'_i - z_{\text{ES}}))|^2 / r_i'^2, \tag{1}$$

$$r'_i = \sqrt{z_{\text{ES}}^2 + (x - x_i)^2 + (y - y_i)^2}, \tag{2}$$

where  $\theta_i$  denotes the phase differences between the  $i$ -th PAA port against port 1.  $\theta_i^{\text{offset}}$  denotes the phase offset at each port. The coordinates  $(x_i, y_i, z_i)$  and  $(x_{\text{ES}}, y_{\text{ES}}, z_{\text{ES}})$  are the port positions of the PAPA elements and the ES position, respectively.

Figure 9 (a) shows a block diagram of the heterodyne

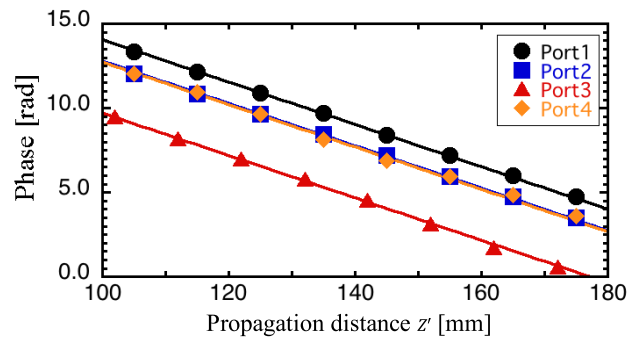


Fig. 8 Measured phase evolution of each port on propagation distance  $z'$  where  $z'$  denotes the propagation distance between swept launcher antenna and patch loop antenna defined by  $\sqrt{x^2 + y^2 + z^2}$ . The coordinates of  $(x, y, z)$  are shown in Fig. 7 (b).

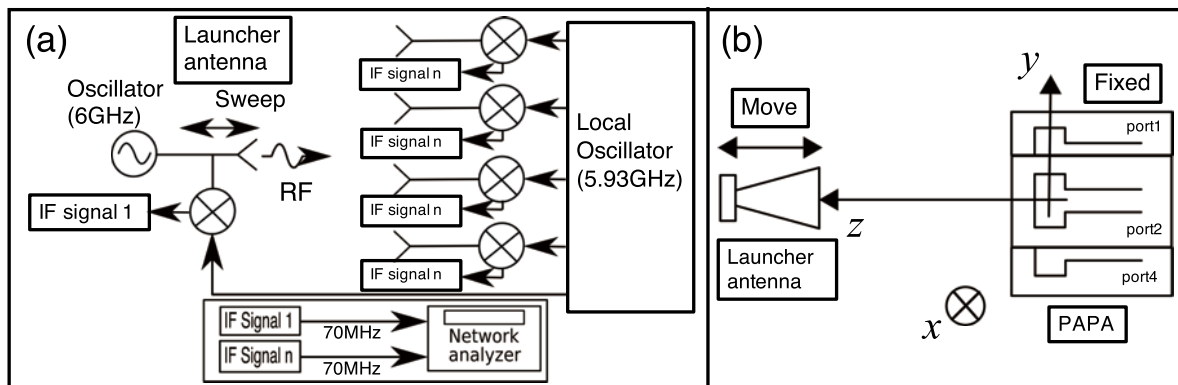


Fig. 7 (a) Block diagram of the heterodyne system with four-element PAPA to observe whether the phase evolution is correctly measured along the propagation for the adaptive array analysis. (b) Configuration to measure the field-phase evolution along the propagation for each element of the PAPA.

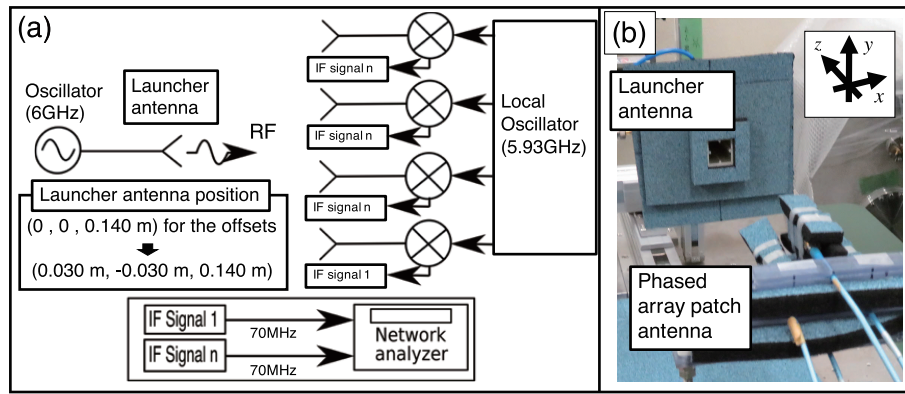


Fig. 9 (a) Block diagram of the heterodyne system with the four-element PAPA to observe whether the emitted-field image from the launcher antenna is 2-dimensionally reconstructed and its emitted source position is properly detected with the adaptive array-analysis. (b) Photo of the launcher antenna and the four-element PAPA. The launcher antenna is located at (0.030 m, -0.030 m, 0.140 m). Here the coordinate origin is the center of the four-element PAPA.

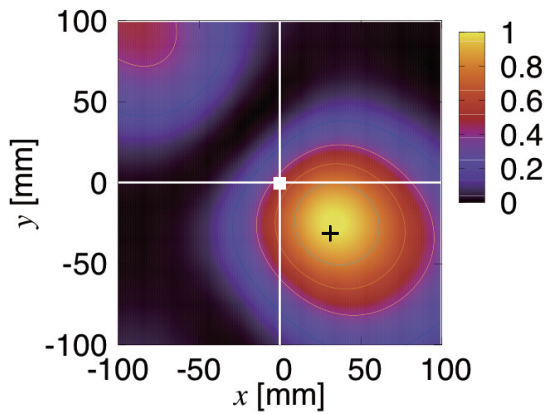


Fig. 10 Field intensity pattern reconstructed through beam-forming analysis for ES radiation from  $(x_{ES}, y_{ES}) = (0.030 \text{ m}, -0.030 \text{ m})$ . The peak point of the reconstructed emission pattern is (0.034 m, -0.024 m).

system on PAPA and the ES source position detection. A photo of the launcher antenna and the four-element PAPA is shown in Fig. 9 (b). Each port phase offsets stemming from the difference among the lengths of the RF circuit were evaluated from the symmetric positions on the four elements for the PAPA center. The launcher antenna was set at  $(x, y) = (0, 0)$ , which is the PAPA center. The coordinate system is defined as shown in Fig. 9 (b). Here, the normal propagating distance from PAPA center to the launcher antenna was  $z = 0.140 \text{ m}$ . The measured phases were described by the phase offsets of the antenna ports. The launcher antenna was re-located at (0.030 m, -0.030 m, 0.140 m), while  $\theta_i$  were measured again. Table 1 summarizes the phase differences between the PAA ports against port 1.

Figure 10 shows the reconstructed emission pattern from equations 1 and 2 with the measured phase after the offset calibration. The cross (+) and closed rectangle (■) denote the ES point and PAPA positions, respectively.

Table 1 Phase differences between the PAA ports against port 1.

port	$\theta_i^{\text{offset}}$	$\theta_i$
port2	25.1 [deg]	23.8 [deg]
port3	-163.3 [deg]	-54.3 [deg]
port4	-4.9 [deg]	76.6 [deg]

Table 2 Phase differences between the PAA ports against port 1 regarding measurement and calculation.

port	measurement ( $\theta_i - \theta_i^{\text{offset}}$ )	calculation
port2	-1.3 [deg]	0.0 [deg]
port3	109.0 [deg]	86.5 [deg]
port4	81.5 [deg]	86.5 [deg]

The peak point of the emission pattern was (0.034 m, -0.024 m) against the ES point of (0.030 m, -0.030 m) in the  $x$  and  $y$  planes. The phase differences between the PAA ports against port 1 could be calculated using  $kz'$ . Table 2 illustrates the list of the phase differences through the measurement and the calculation. The measured phases were in good agreement with the calculation except for the port 3. Since the patch antenna was fixed only with SMA cabling in the setting of PAPA, port 3 would be misaligned because of gravity while conducting the experiment. The proper fixtures for PAPA are required in our future works.

Consequently, the location of ES can be properly identified through 2D image reconstruction with the prototype PAPA. The proof-of-principle of the prototype PAPA was successfully shown, proving that the 2D image reconstruction with multi-element PAPA is feasible.

## 4. Conclusions

The fabricated patch loop antenna is simple and compact. It also has an advantage for practical mass produc-

tion. The fabricated patch antenna can measure the phase profile and evolution properly at the low-power bench test. The prototype PAPA comprised four-elements, in which the distance between the antennae is 60 mm was assembled. The 2D imaging measurement was demonstrated using the four-elements PAPA. The ES position could be detected within a few mm range when the ES was located at the normal propagating distance of  $z = 0.140$  m.

## Acknowledgments

This research was partially supported by Grant-in-Aid for Challenging Exploratory Research (JSPS KAKENHI Grant Number JP16K14529).

- [1] H.P. Laqua *et al.*, Phys. Rev. Lett. **78**, 3467 (1997).
- [2] H. Idei *et al.*, J. Plasma Fusion Res. Series **8**, 1104 (2009).
- [3] H. Idei *et al.*, J. Instrum. **11**, 4, C04010 (2016).
- [4] K. Mishra *et al.*, Rev. Sci. Instrum. **85**, 11E808 (2014).
- [5] A. Pal *et al.*, IEEE Trans. Antennas Propag. **65**, 576 (2017).